Discrete numerical modeling of granular materials considering crushability

QIAN Jian-gu (iD) http://orcid.org/0000-0001-9639-3627; e-mail: qianjiangu@tongji.edu.cn

GU Jian-bo (iD) http://orcid.org/ 0000-0002-0130-5565; e-mail: gujianbo@tongji.edu.cn

GU Xiao-qiang* (iD) http://orcid.org/000-0002-2010-6510; ✉ e-mail: guxiaoqiang@tongji.edu.cn

HUANG Mao-song (iD) http://orcid.org/0000-0002-1990-6641; e-mail: mshuang@tongji.edu.cn

* Corresponding author

Key Laboratory of Geotechnical and Underground Engineering of Ministry of Education, Tongji University, Shanghai 200092, China

Department of Geotechnical Engineering, Tongji University, Shanghai 200092, China

Abstract: The aim of this study is to numerically investigate the influence of particle breakage on the mechanical behavior of granular materials using a discrete element method (DEM). To enable particle crushing, non-crushable elementary particles are boned together to represents the granular aggregates which can be crushed when the external force exceeds its strength. The flaw of the aggregate was also modeled by randomly distributed void. Single particle crushing tests were carried out to determine the distribution of particle strength. The results of single particle crushing tests illustrate that the simulated single particle fracture strength and pattern agree well with the Weibull's distribution equation. Conventional oedometer tests, drained monotonic and cyclic triaxial tests were also carried out to investigate the crushing of the aggregates and the associated mechanical behaviors. The effect of confining pressure on the crushing of aggregates and the mechanical behavior was also analyzed. It was found that the peak stress and dilation decrease significantly when particle crushing was considered. The deformation behavior of the specimen is essentially controlled by two factors: particle rearrangement - induced dilation and particle crushing - induced contraction. The increase of permanent strain and the reduction of dilation were observed during cyclic loading and they tend to reach a stable state after a certain number of cycles. The crushing of aggregate is most significant in the first two cycles. The results also indicated that for the same axial strain the volumetric strain and the bound breakage in the cyclic loading tests are significantly larger than that in the monotonic loading tests, especially at high cyclic stress ratio.

Keywords: DEM simulation; Granular materials; Crushing; Monotonic and Cyclic triaxial test

Introduction

Since the 1970s, many high dams over 100m have been built in the mountain regions of China. For these dams, granular materials are subjected to extremely high confining pressure. In addition, granular materials will undergo both static loading during construction and cyclic loading during post-construction when the water level of dam varies repeatedly or during earthquakes. It is well agreed

that the mechanical behavior of granular materials, such as strength and deformation, is very complex. Therefore, it is still a big challenge to model their behavior for safety assessments of these dams.

From a mechanical perspective, the complex behaviors of granular material result from the inherently particulate and heterogeneous nature of the medium. Many experimental and numerical research studies have been conducted on the single particle crushing and the mechanical behavior of crushable soils. It has been found that a number of factors will affect the degree of particle crushing and the major ones include the grading, grain shape, the strength of grains and the applied stress. However, it is difficult to monitor the evolution of particle crushing during the experimental test and reveal the fundamental crushing mechanism.

Granular materials are inherently discrete and very suited to be modeled by the discrete element method (DEM), which was originally proposed by Cundall and Strack (1979). It has been well recognized as a powerful tool to investigate different mechanical behaviors of granular materials at a particulate level (Thornton 2000; Qian et al. 2011; Qian et al. 2013a, b; Gu et al. 2013, 2014), although its computational cost is very high and not suitable for large boundary value problems. Robertson (2000) simulated the crushable aggregates composed of elementary balls in hexagonal close packing (HCP) bonded together by contact bonds. McDowell and Harireche (2002a, b) proposed a procedure to create aggregates of different sizes with crushing strengths that obey Weibull (1951) statistics. Deluzarche and Cambou (2006) modeled the crushable particle using breakable clusters of two-dimensional (2D) balls, which made it possible to model the crushing in a simple way and allowed the discrete structure of material to be taken into account. Bolton et al. (2008) investigated the micro and macro-mechanical behavior of crushable particles. Wang and Yan (2011, 2013) proposed a new method to generate aggregates and investigated the macro- and micro-mechanical behaviors of crushable soils under plane strain conditions.

Ueda et al. (2013) investigated the effect of particle shape on the compression behavior of granular materials, and divided the crushing into three types according to the single particle crushing tests on elliptical particles. The crushing of particle can also be modelled by replacing particles fulfilling a predefined failure criterion with smaller, self-similar fragments. Astrom and Herrmann (1998) used the self-similar fragments to replace the 'broken' particles and studied the mechanical behavior of two-dimensional granular medium under pressure. Tsoungui et al. (1999) proposed a theoretical model to define the failure criterion on an individual grain subjected to an arbitrary set of contact forces and investigated the crushing mechanisms of grains inside a granular material under one-dimensional compression. Based on the work of Tsoungui et al. (1999), Lobo-Guerrero et al. (2005) implemented a new simplified tensile failure criterion in the DEM and studied the penetration resistance of driven piles. McDowell and Bono (2013, 2014) incorporated a simple breakage mechanism and investigated the nature of crushing and its effects on the critical state behavior. In addition, combined finite element method (FEM) and DEM have been developed to model the continuum-discontinuum systems under a uniform framework. Munjiza et al. (1995, 2004) proposed a combined finite-discrete element method that applied to a wide range of engineering and scientific problems. Owen et al. (2004) presented an integrated discrete-finite element simulation strategy for modelling practical problems characterized by multi-fracture and discrete phenomenon. Xiang et al. (2009) developed an efficient ten-nodded quadratic element to improve the accuracy of simulation caused by locking problems associated with linear tetrahedral finite element. Zhou et al. (2015) investigated the influence of particle crushing and shape on the mechanical behavior of granular materials by FDEM method.

In this paper, three-dimensional aggregates are used to simulate the crushable particles. Both the macro- and micro- mechanical behaviors of granular soils in the oedometer tests, drained monotonic and cyclic triaxial tests are investigated. The work aims to gain an insight into understanding effects of grain crushing on the one-dimensional compression, monotonic and cyclic shear responses under different confining pressures. The crushing effects are highlighted by comparing the results of crushable and uncrushable specimens.

1 Single Particle Crushing Test

The well recognized commercial software PFD3D was used to perform the numerical discrete element method modeling. In DEM, the soil particles interacted at their contacts. The interaction between contacts was controlled by the contact law and the motions of the particles were controlled by the Newton's second law. By an explicit central differential algorithm, the particle positions, particle contact forces and the particle motions are updated alternatively. Details of the PFC3D can be found in the manual of the software. In this study, the soil particle is modelled as an aggregate of many mono-sized elementary balls in hexagonal close packing and they are bonded together by parallel contacts. Note that the aggregate can be crushed, while the elementary ball cannot be crushed in the simulation. The diameters of the aggregates are ranged between 1mm and 2mm, and the diameter of elementary ball is 0.2mm. The parallel bonds are installed at all the contacts existing between elementary balls. Generally, the contact bond model which was widely employed in previous DEM investigations on particle crushing is unable to simulate the rotational resistance. However, due to the absence of the rotational resistance, the contact bond model frequently results in the loss of a visible physical fracture of aggregate (Wang and Yan 2011). On the other hand, the parallel bonds can transmit both forces and moments between particles, while contact bonds can only transmit forces acting at the contact point. The parameters used in the DEM simulation are listed in Table 1. During the test the bond breaks if the contact force at a contact exceeds the bond strength. To achieve the

statistical variation of the strength, a certain number of the elementary balls in an aggregate were randomly removed based on trial and error.

McDowell and Amon (2000) shown that the fracture strength of soil particles essentially obeys the Weibull's statistical distribution (Weibulll 1951) given by:

$$P_s = \exp\left[-(\frac{\sigma}{\sigma_0})^m\right] \qquad (1)$$

where σ_0 is the characteristic stress at which 37% of particles survive and m is the Weibull modulus which decreases with increasing variability in strength. The survival probability P_s is calculated using the mean rank position as:
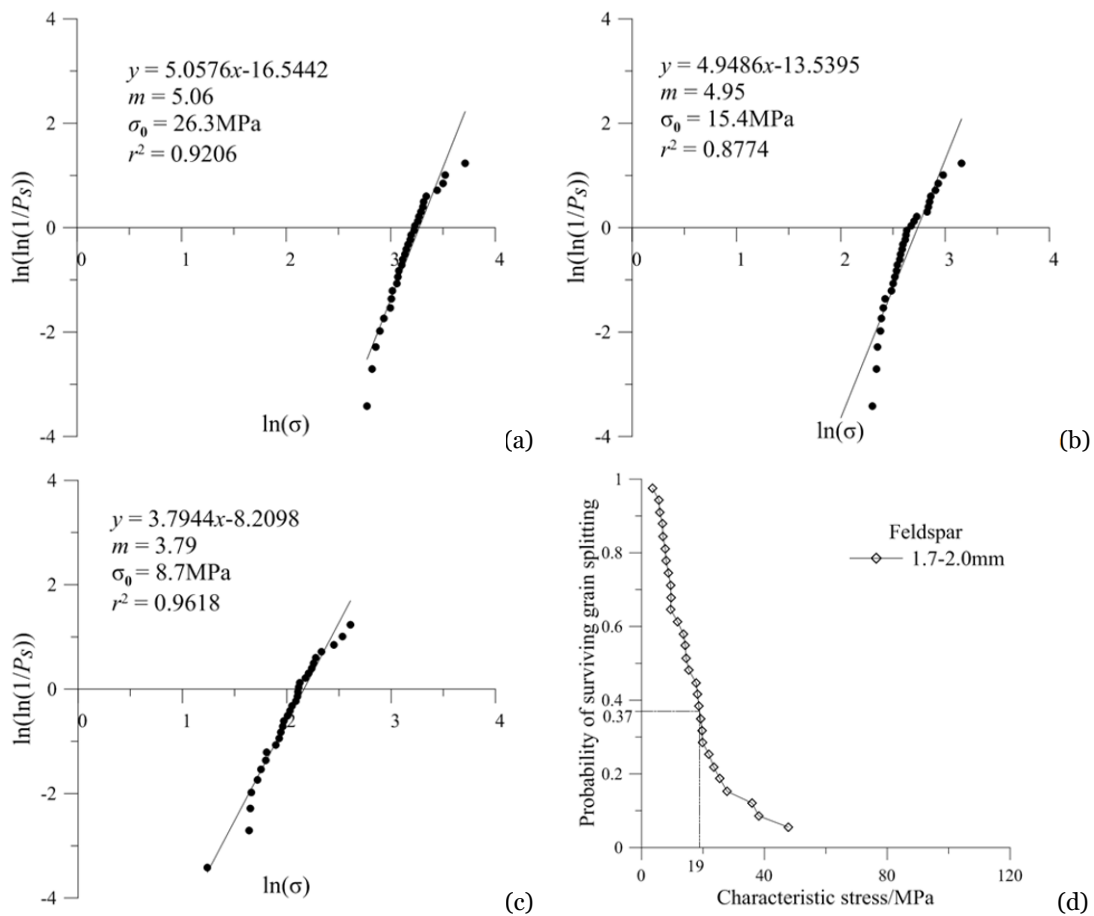
$$P_s = 1 - \frac{i}{N+1} \qquad (2)$$

where i is the rank position of a grain when sorted into increasing order of peak stress, and N is the total number of grains. Eq.(1) can then be rewritten as:

$$\ln\left[\ln\left(\frac{1}{P_s}\right)\right] = m \cdot \ln(\sigma) - m \cdot \ln(\sigma_0) \qquad (3)$$

The parameters m and σ_0 can be obtained by fitting technique based on the results of single particle crushing tests.

Figure 1 shows the results of Weibull probability for 2mm diameter aggregates under different removal percentages. The removal percentage is defined as the percentage of the removed elementary balls in an aggregate before single particle crushing test. As the removal percentage increases, the Weibull modulus and characteristic stress decreases as expected, which indicates the decrease of particle strength. Aggregates with 30% removal of elementary balls are used in the following tests according to the following reasons: (1) laboratory test results by Ashby and Jones (1986) showed that materials such as chalk, brick, stone, pottery and cement have $m \approx 5$, while engineering ceramics such as Al_2O_3, SiC have $m \approx 10$; (2) Figure 1(d) shows the laboratory test results on Feldspar with diameter between 1.7mm-2.0mm and the characteristic stress for Feldspar is about 19MPa. The characteristic stress in the DEM simulation on the aggregate with 30% removal of ball is 15.4MPa, which is close to the results of Feldspar.

Table 1 Parameters of elementary balls and parallel bonds

Diameters of aggregate (mm)	1.0-2.0
Diameter of elementary ball (mm)	0.2
Density of ball (kg/m³)	2650
Normal and shear stiffness of ball (N/m)	2×10^6
Friction coefficient of ball	0.5
Normal and shear parallel bond strength (N/m²)	3×10^8
Normal and shear parallel bond stiffness (N/m³)	3×10^{14}
Wall stiffness (N/m)	1×10^{10}

Figure 1 Weibull probability for 2mm diameter aggregate for: (a) 20% removal of elementary balls; (b) 30% removal of elementary balls; (c) 40% removal of elementary balls; (d) Laboratory tests for Feldspar by Nakata et al. (1999).

Figure 2 shows the typical results of two aggregates with a 2mm diameter in single particle crushing tests in the DEM simulation, together with the laboratory results on quartz sand particle and feldspar particles by Nakata et al. (1999). No elementary balls are removed in one aggregate and the other is removed about 30% of elementary balls. The aggregate without ball removal (i.e. 0% ball removal) contains a total number of 527 balls. It is interesting to note that the response of the aggregate without removal of elementary balls has only one peak in the force-displacement curve. The peak value is about 300N at a displacement of 0.075mm. However, the response of the aggregate with 30% removal of elementary balls has several peaks and the peak value is only about 40N at a displacement of 0.27mm, much lower than that of the aggregate without removal of elementary balls as expected. Figure 2(b) and 2(e) show the photographs of a quartz particle and a feldspar

particle after testing made by Nakata et al. (1999). The quartz particle tended to break into just two or three pieces, while the feldspar particle shattered into many smaller pieces. The saw-tooth curve of the feldspar could be explained by the particle corners fractured before final catastrophic fracture. It is interesting to note that the observation of particle breakage pattern in DEM is similar as the results in laboratory tests (see Figure 2(c) and Figure 2(f)).

2 One-dimensional Compression Test

2.1 General description

The dimensions of DEM specimen are $10 \times 10 \times 10 mm^3$. For each specimen, a certain number of initial 'exo-sphere' are first created in the specimen and then they are cycled to
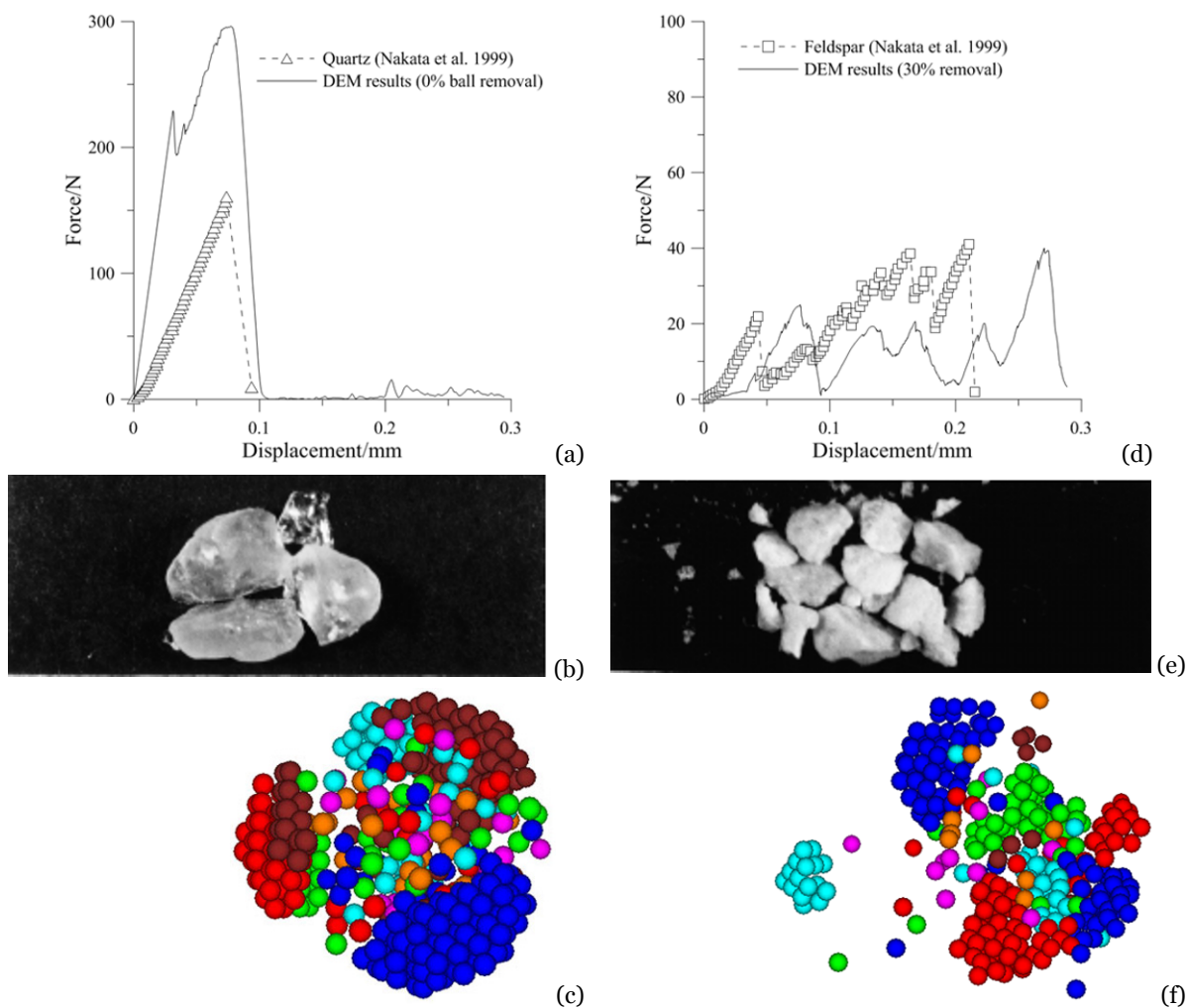
Figure 2 Crushing test on a 2mm aggregate: (a) stress-displacement relationship of the aggregate without ball removal; (b) photograph of a quartz particle after crushing test; (c) crushing of the aggregate without ball removal; (d) stress-displacement relationship of this aggregate with 30% ball removal; (e) photograph of a feldspar particle after crushing test; (f) crushing of the aggregate with 30% ball removal.

equilibrium (Figure 3(a)). When the specimen reaches the equilibrium, the exo-sphere is deleted and an aggregate is created just in the center of the deleted exo-sphere and with the same diameter (Figure 3(b)). When the replacement is finished, the specimen composed of crushable aggregates without removal of elementary ball is generated (Figure 3(c)). The generated specimen is cycled again to equilibrium and the specimen is in a dense state. When the replacement is finished, the specimen composed of crushable aggregates without removal of elementary ball is generated (Figure 3(c)). The generated specimen is cycled again to equilibrium and the specimen is in a dense stateIn order to achieve the required statistical distribution of crushing strength, around 30% of elementary balls in an aggregate are moved randomly and the specimen is cycled to equilibrium again to generate the final specimen (Figure 3(d)). This process of specimen generation is similar as that by Cheng et al. (2003, 2004). The final specimen is composed of 524 nearly round aggregates with diameters ranged from 1mm to 2mm. Then the top and bottom walls move closer to compress the sample, while the lateral walls are fixed, mimicking the one-dimensional compression in oedometer tests.

2.2 Results of one-dimensional compression tests

Figure 4(a) shows the compression curve in V/V_o-logσ space, where V is the current sample volume and V_o is the initial sample volume. It is
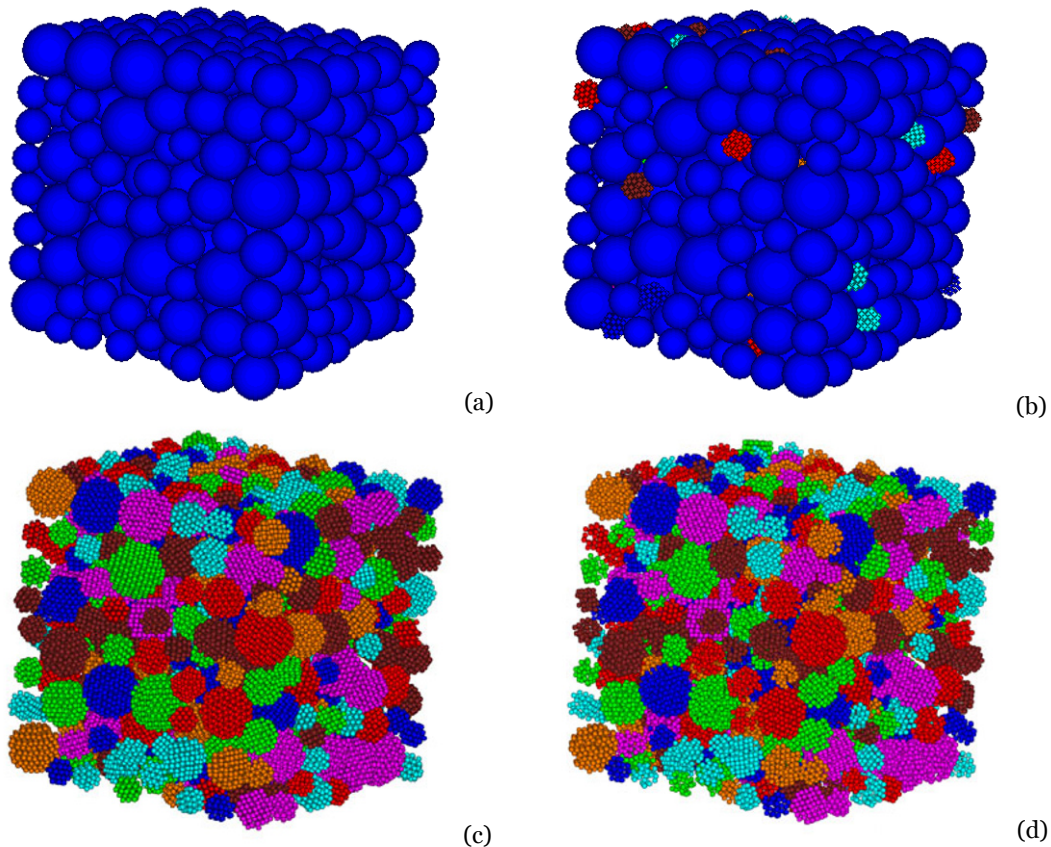
Figure 3 Schematic of specimen generation: (a) Initial specimen; (b) Ball replaced by aggregate; (c) Specimen composed of crushable aggregates without removal of elementary ball; (d) Specimen composed of crushable aggregates with removal of 30% elementary ball.

difficult to use the void ratio e, because each soil particle is modelled as a porous aggregate, and when aggregates broke, internal voids become external voids. There is a significant decrease in volume ratio at the beginning of compression test. This is due to the rearrangement of aggregates, because around 30% of elementary balls are removed and it leaves a large void between aggregates. As seen in Figure 4(a), yielding appears to occur around 1MPa, at which the ratio of volume decreases significantly with increase pressure. This can be proved by Figure 4(b), which shows the relationship between bond breakage and volumetric strain. When the volumetric strain exceeds 23% corresponding to a vertical stress of 1MPa, the rate of bond breakage increases sharply. Beyond yield an approximately linear normal compression line could be observed. Figure 4(d) shows the evolution of particle size distributions of the specimen. There is an obvious gap between the particle size distribution curve at 1000kPa and 1500kPa, which indicates that significant crushing

occurs after 1MPa. The effective grain size is defined as follow:

If the aggregate composes N elementary balls, the effective grain size D is the diameter of the sphere which has the same volume as the total volume of N elementary balls, that is:

$$\frac{1}{6}\pi D^3 = N \cdot \frac{1}{6}\pi d^3 \tag{4}$$

Eq.(4) can then be rewritten as:

$$D = \sqrt[3]{N} \cdot d \tag{5}$$

Note that the effective grain size does not account for the gaps between elementary balls and the shape of each aggregate. There is a large gap between the particle size distributions at σ_z=1000kPa and σ_z=1500kPa, this is due to the large number of particle break at 1MPa and this observation once again proves that the yielding stress is around 1MPa.

3 Drained Triaxial Tests under Monotonic and Cyclic loading

3.1 General description

Before the drained triaxial test, the specimen is isotopically consolidated to the stress states of 200, 400, 600, 800, 1000, 1500 and 2000kPa by

servo control of the boundary walls. Note that the specimen is the same one in the one-dimensional compression test. During isotropic consolidation, the six walls move inward to compress the sample and the displacement of the wall in each calculation step is determined by the stress difference between the current value and the aimed value as well as the average contact stiffness between the walls and balls. After a large number of calculation steps, the specimen can reach a designated stress. The results of isotropic compression test are shown in Figure 5. The V/V_0-mean effective stress curve in Figure 5(a) and bond breakage percent-confining stress curve in Figure 5(b) also support the conclusion that the yielding stress of the specimen is at around 1MPa. Figure 5(c) shows the evolution of particle size distribution under different isotropic confining stresses. As the confining stress increases, the small particle fragments lies in the range between 0.2mm and 0.6mm increases significantly, which are generated from the crushing of large particles.
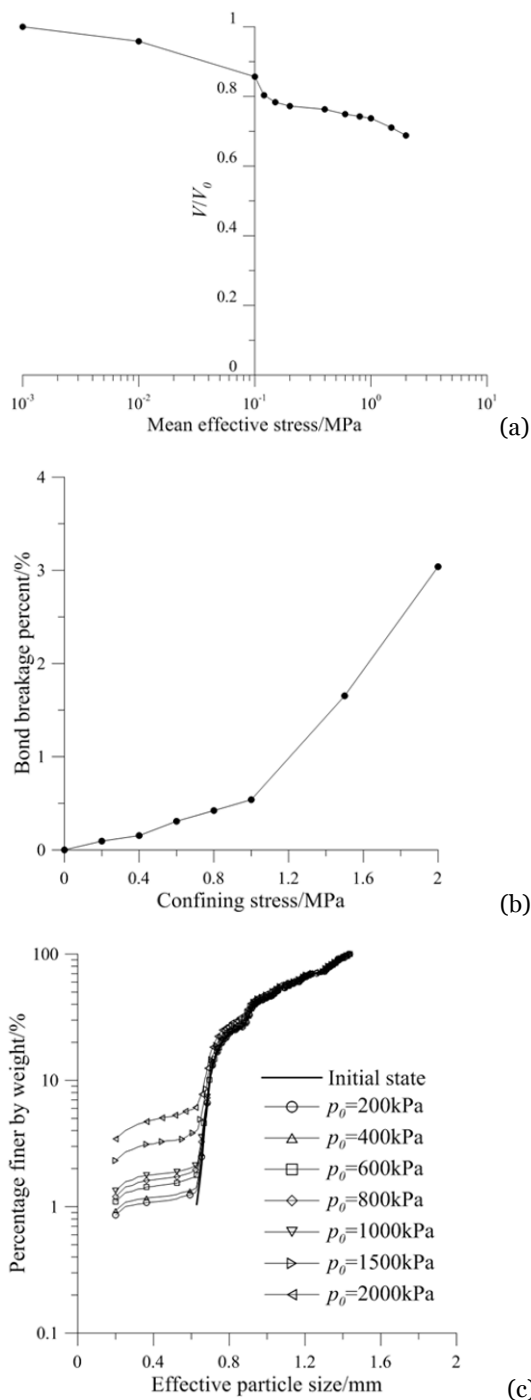
After consolidation, drained monotonic and cyclic triaxial tests are carried out to investigate the mechanical behavior of aggregates. During the triaxial tests, the top and the bottom walls moved at a constant rate of 0.05m/s to compress the specimen, while the lateral stress is maintained using servo controls of lateral walls. The term "drain" means the constant effective lateral stress which is the same as in a conventional laboratory triaxial test, although the specimen is dry in the DEM simulation. The maximum axial strain is 20% in monotonic tests. Meanwhile, the cyclic test is a kind of stress-controlled test and the controlled stress ratio q/p ($q=\sigma_1-\sigma_3$, $p=(\sigma_1+\sigma_2+\sigma_3)/3$) is ranged from 0.6 to 1.2.

For better comparison, another two types of grains, a crushable grain without removal of elementary ball (a crushable grain without flaw) and an uncrushable grain without removal of
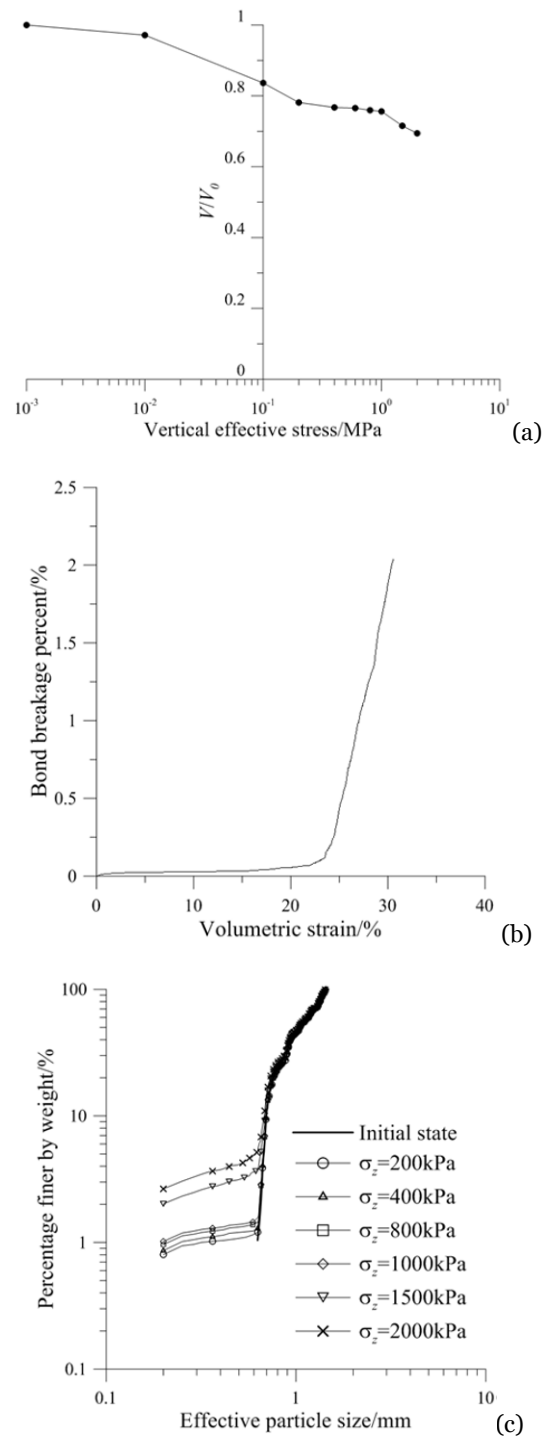
Figure 4 Results of one-dimensional compression test: (a) Volume ratio versus vertical effective stress; (b) Bond breakage percent versus confining stress; (c) Evolution of particle size distribution.

elementary ball (an uncrushable grain without flaw) are also used in the simulation. Note that the place of each grain in these specimens is exactly the same in the DEM simulation.

(a)

(b)

(c)

Figure 5 Results of isotropic consolidation: (a) Volume ratio versus mean effective stress; (b) Bond breakage percentage versus confining stress; (c) Evolution of particle size distribution.
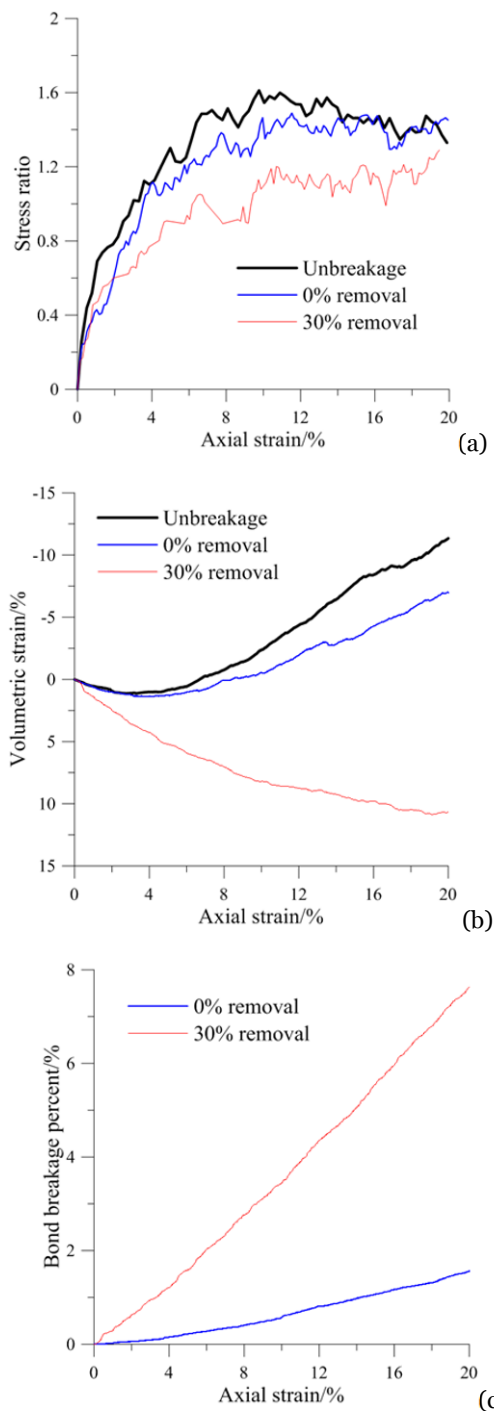
3.2 Results of drained monotonic triaxial tests

Figure 6(a) shows the stress ratio q/p versus axial strain for specimens with different aggregate characteristics at an initial confining pressure of 1000kPa. It is clear that the shear stress of the specimen with uncrushable particles reached a peak first and then decreases with increasing axial strain, indicating a strain softening behavior. However, the shear stress of specimens with crushable particles increases with increasing axial stress, indicating a hardening behavior. As seen in Figure 6(b), the specimens with uncrushable particles and crushable particle without flaw illustrate dilative behavior, while the specimen with crushable particles with flaw shows contractive behavior. To clarify this point, the bond breakage percent, defined as the ratio of the number of broken bonds to the total number of bonds is shown in Figure 6(c). The bond breakage percent increases as the axial strain increases, but the degree of bond breakage is much more significant in the specimen of crushable particles with flaw. It also reveals that the particle crushing significantly affect the dilatancy of the specimen and therefore the mechanical behavior. For the crushable soil, the fragment of aggregate may fill up the voids between large aggregate and result in volume contraction and therefore a hardening behavior.

Figure 7 shows the deviatoric stress and the volumetric strain of the specimens with 30% ball removal aggregate at various confining pressures. As seen in Figure 7(a), the deviatoric stress generally increases with axial strain, although some fluctuation was observed. For higher initial confining pressure, the initial stiffness and the peak deviatoric of the specimen are higher as expected. The specimen shows strain softening behavior at low confining pressures, while showing strain hardening behavior at high confining pressures. Figure 7(b) clearly showed that at low confining pressure, an overall dilative behavior in shearing is observed in the specimen although a certain amount of particle breakages may also happen during shear, as indicated in Figure 6(c). As the confining stress increases, the particle crushing increases and the related volume contraction is much larger than the dilation from particle rearrangement, resulting in an overall contractive behavior. These results convincingly indicate the importance of accounting for particle crushing in modeling the mechanical behavior of crushable soils.
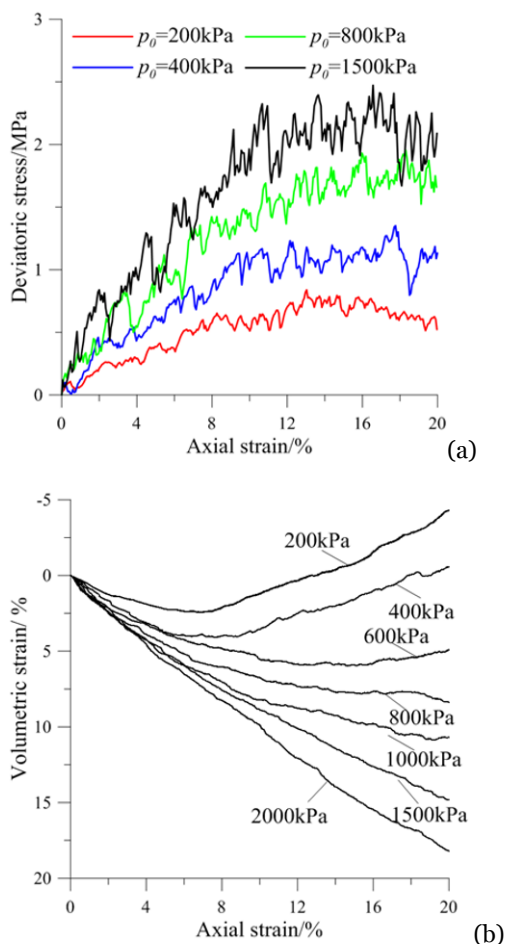
For validation the DEM simulation, the laboratory results on crushable aggregates by Kong et al. (2009) are shown in Figure 8. It is clear that the specimen also shows strain softening and dilative behaviors at low confining pressures, while showing strain hardening and contractive behaviors at high confining pressures. It convincingly illustrates that the trend of results in DEM and laboratory tests agree with each other.

Figure 9(a) shows the evolution of particle size distribution during the shearing under a confining stress of 1000kPa. It is clear to see that, as the axial strain increases, the small particle fragment within the range between 0.2mm and 0.6mm increases significantly. The grading curves keep concave and rotate clockwise around the maximum particle size. Figure 9(b) compares the grading curves at the axial strain of 20% under various confining pressures. As the confining pressure increases, the percent of small particle fragment increases, and there is a tendency towards a potential stable grading curve. It may be deduced that a linear particle size distribution in a double logarithmic graph can be obtained as the confining pressure

(a)

(b)

(c)

Figure 6 Drained triaxial test under monotonic loading: (a) Stress ratio q/p versus axial strain; (b) Volumetric strain versus axial strain; (c) Bond breakage percentage versus axial strain at the confining stress of 1000kPa.

(a)

(b)

Figure 7 Drained monotonic triaxial test in DEM simulation: (a) Deviatoric stress versus axial strain; (b) Axial strain versus axial strain.
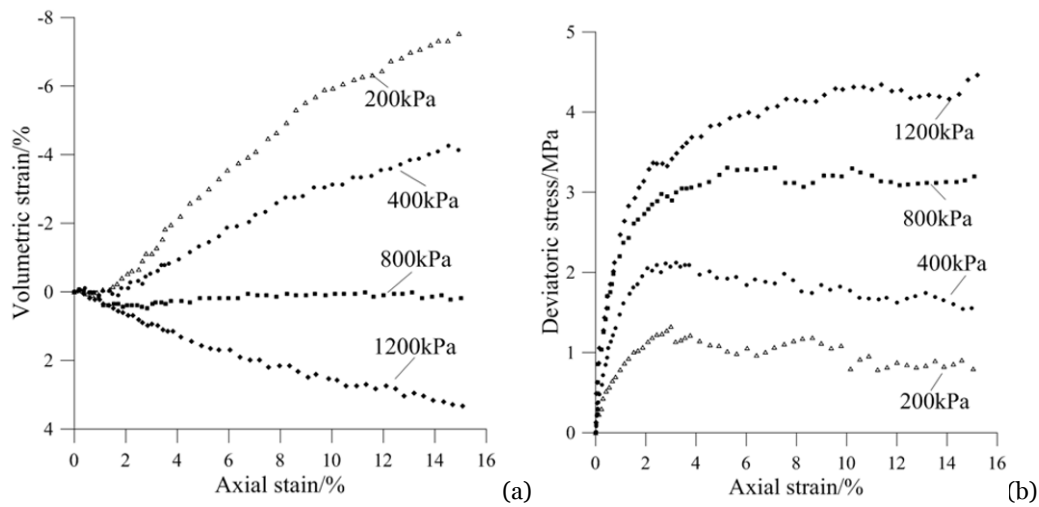
Figure 8 Drained monotonic triaxial test in laboratory by Kong et al. (2009): (a) Deviatoric stress vsersus axial strain; (b) Axial strain versus axial strain.
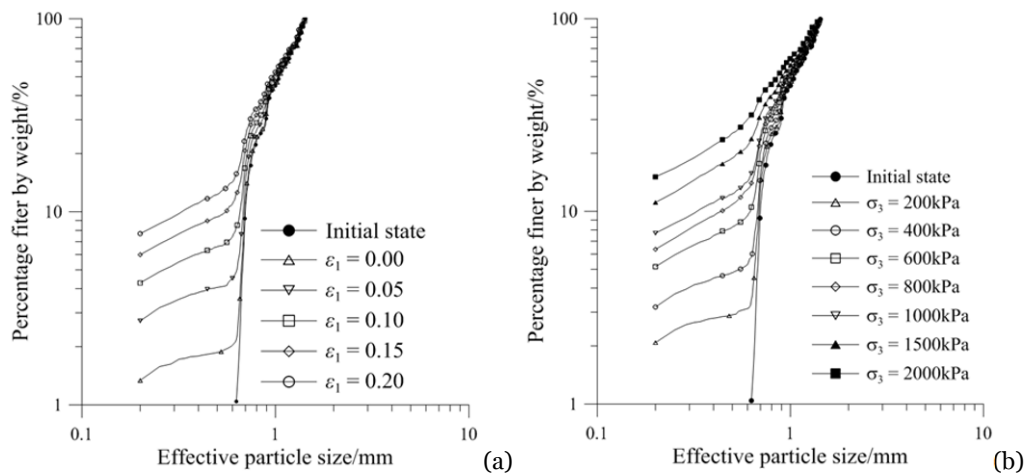
Figure 9 Evolutions of particle size distributions of crushable specimens: (a) Specimen with 30% removal of elementary ball under confining stress of 1000kPa; (b) Specimen with 30% removal of elementary ball under various confining stresses at 20% axial strain.

further increases. This observation is similar to those made by Wang and Yan (2013).

3.3 Results of cyclic triaxial tests

Figure 10(a) shows the hysteresis loops for the first 5 cycles for the specimen of particles with 30% removal of elementary balls under a cyclic stress ratio of 0.8. It can be noted that the axial strain in the 1st cycle is much larger than those occur in the subsequent cycles. During the first cycle, large non-recoverable or permanent deformation happens, but the non-recoverable component decreases as the number of cycles increases, representing an increase of cyclic stiffness. It is consistent with the

laboratory observations on the accumulation of permanent deformation of sand (Wichtmann et al. 2007). As seen in Figure 10(b), the induced permanent deformation is the result of particle rearrangement and particle crushing (see Figure 6). It also indicates that there is still a small amount of bond breakage occuring during unloading of each cycle, compared to that during the loading. However, as the number of the cycle increases, the percentage of bond breakage tends to toward a potential stable condition, which means no breakage will happen after a sufficient number of loading cycles. To illustrate such a tendency, Figure 10(c) shows the evolution of particle size distribution at the end of each loading-unloading

cycle. As the number of cycle increases, the difference between two particle size distribution (PSD) curves becomes smaller, which means the crushing of particles tends to stop. Figure 10(d) shows the relationship between accumulated strain at end of each cycle and the number of cycle. It is obvious that after 100 cycles, all the accumulated strains tend to be stable. Here the shear strain ε_q is defined as:

$$\varepsilon_q = \frac{2}{3}(\varepsilon_1 - \varepsilon_3) \qquad (6)$$

Figure 11 compares the results of drained cyclic triaxial test at different stress ratio. It is obvious that the volumetric strain increases as the stress ratio increases. However, it should be noted that the interval between volumetric strain at stress ratio of 1.0 and 1.2 is much larger than those at other adjacent stress ratios. It can be deduced that the particle breakage at the stress ratio of 1.2 is much larger than that at the other stress ratios. For better illustration, the bond breakage percentage is plotted against the number of cycles at different

cyclic stress ratios in Figure 11(b). It convincingly indicates the increment of bond breakage percentage at stress ratio of 1.2 is much larger than those at other stress ratios. It seems that the specimen has its own critical failure point, when the axial deviatoric stress exceed this point, it will cause a lot of particle breakage. However, as the small break fragments fill in the void between particles, the strength of specimen increases, which results in a tendency that the soil becomes stable as the number of cycle increases.

Figure 12 compares the volumetric strain and the bond breakage in the monotonic loading tests and cyclic loading tests. Note that the axial strain in the cyclic strain means the accumulative axial strain curtain number of cyclic loads. As seen in Figure 12, for the same axial strain, the volumetric strain is much larger in cyclic loading than that in the monotonic loading, especially for large cyclic stress ratio. Such phenomenon is mainly due to the more significant bond breakage in cyclic loading, as indicated in Figure 12(b).
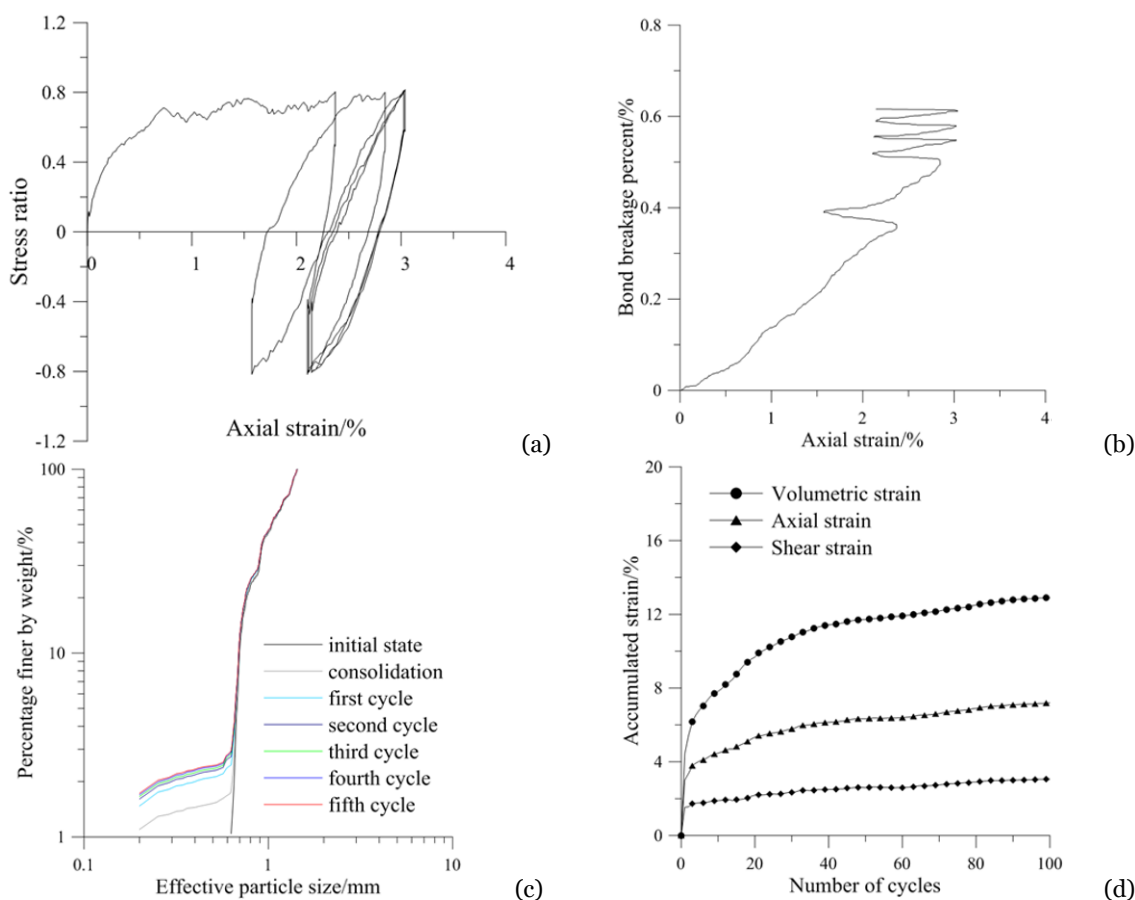

Figure 10 Drained triaxial test under cyclic loading: (a) Stress ratio q/p versus axial strain; (b) Bond breakage versus axial strain; (c) Evolution of particle size distribution; (d) Accumulated strains versus number of cycles.

4 Conclusions

This paper investigated the effects of particle breakage on the mechanical behavior of crushable particles under one-dimensional compression, drained monotonic triaxial loading and cyclic triaxial loading. The statistical variation of the single particle fracture strength is achieved by randomly removing about 30% of elementary balls which compose the aggregates. The result illustrates that the simulated single particle fracture strength agrees well with the Weibull's distribution equation. The Weibull modulus *m* of the aggregates with 30% removal of balls is 4.95 and the characteristic stress is 15.4 MPa. It is shown that a major splitting behavior is observed for the particle without ball removal. However, for the aggregates with 30% removal of balls, several peaks in the force-displacement curve can be observed.

It is clear that the deformation behavior of a dense granular specimen is essentially controlled by two factors: particle rearrangement-induced dilation and particle crushing-induced contraction. For crushable dense specimens, the confining stress plays a critical role on the volumetric strain behavior. Under low confining stresses, overall dilation is still observed but is much less than that of the uncrushable specimen. Under high confining stresses, the specimens become contractive. It seems that the final particle size distribution of the crushable specimen tends to reach a linear distribution in a double logarithmic.

In cyclic triaxial tests, the accumulated strains after each cycle (include axial strain, shear strain and volumetric strain) is most significant in the first several cycles. The induced permanent deformation is mainly due to the particle crushing.
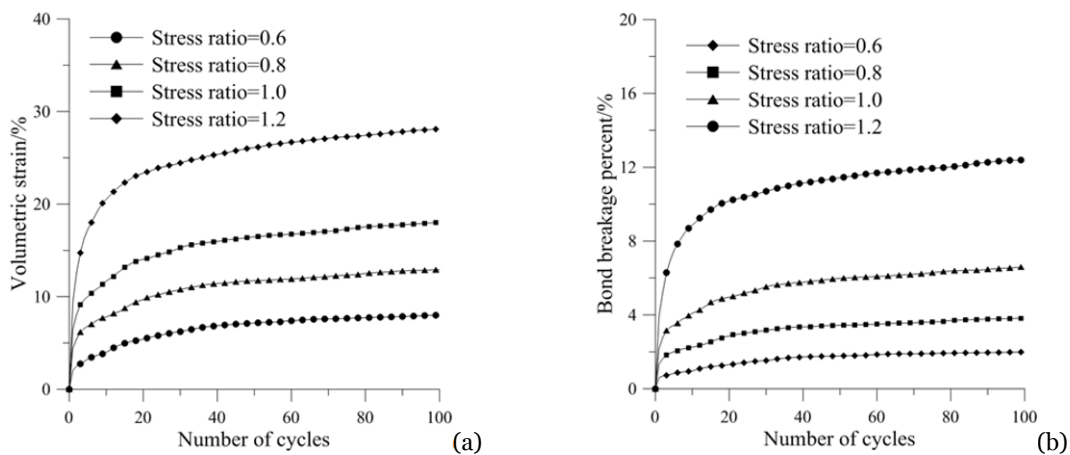
Figure 11 Drained cyclic triaxial tests at different stress ratios: (a) Volumetric strain versus number of cycles; (b) Bond breakage versus number of cycles.
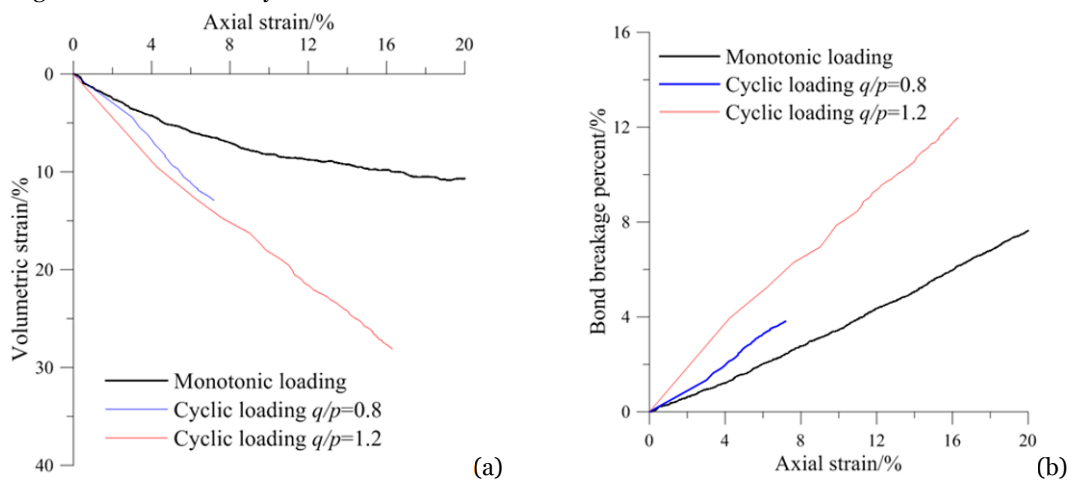
Figure 12 Comparison of results between monotonic loading and cyclic loading: (a) Volumetric strain versus axial strain; (b) Bond breakage versus axial strain.

The percentage of bond breakage trends to a potential stable condition as the number of the cycle increases, which means the accumulated strains tend to be stable accompanied an increasing cyclic stiffness. For the same axial strain, the volumetric strain is much larger in cyclic loading than that in the monotonic loading, especially for large cyclic stress ratio.

References

Ashby MF & Jones DRH (1986) Engineering materials 2. Pergamon Press, Oxford.

Åström JA, Herrmann HJ (1998) Fragmentation of grains in a two-dimensional packing. The European Physical Journal 5(3): 551-554. DOI: 10.1007/s100510050476

Cheng YP, Nakata Y, Bolton MD (2003) Distinct element simulation of crushable soil. Géotechnique 53(7): 633-641. DOI: 10.1680/geot.2003.53.7.633

Cheng YP, Bolton MD, Nakata Y (2004) Crushing and plastic deformation of soils simulated using DEM. Géotechnique 54(2): 131-141. DOI: 10.1680/geot.2004.54.2.131

Cundall PA, & Strack ODL (1979) A discrete numerical model for granular assemblies. Géotechnique 29(1): 47-65. DOI: 10.1680/geot.1979.29.1.47

Deluzarche R, and Cambou B (2006) Discrete numerical modelling of rockfill dams. International Journal for Numerical and Analytical Methods in Geomechanics 30(11): 1075-1096. DOI: 10.1002/nag.514

Gu XQ, Yang J, Huang MS (2013) DEM simulations of the small strain stiffness of granular soils: effect of stress ratio. Granular Matter 15(3): 287-298. DOI: 10.1007/s10035-013-0407-y

Gu XQ, Huang MS, Qian JG (2014) DEM investigation on the evolution of microstructure in granular soils under shearing. Granular Matter 16(1): 91-106. DOI: 10.1007/s10035-013-0467-z

Kong DZ, Zhang BY, Sun X (2009) Triaxial tests on particle breakage strain of artificial rockfill materials. Chinese Journal of Geotechnical Engineering 31(3): 464-469.

Lobo-Guerrero S, Vallejo LE (2005) Crushing a weak granular material: experimental numerical analyses. Géotechnique 55(3): 245-249. DOI: 10.1680/geot.2005.55.3.245

Nakata Y, Hyde AFL, Hyodo M, Murata H (1999) A probabilistic approach to sand particle crushing in the triaxial test. Géotechnique 49(5): 567-583. DOI:10.1680/geot.1999.49.5.567

McDowell GR, Bolton MD (1998) On the micro mechanics of crushable aggregates. Géotechnique 48(5): 667-679. DOI: 10.1680/geot.1998.48.5.667

McDowell GR, Amon A (2000) The application of Weibull statistics to the facture of soil particles. Soils Found 40(5): 133-141. DOI: 10.3208/sandf.40.5_133

McDowell GR, Harireche O (2002a) Discrete element modelling of soil particle fracture. Géotechnique 52(2): 131-135. DOI: 10.1680/geot.2002.52.2.131

McDowell GR, Harireche O (2002b) Discrete element modelling of yielding and normal compression of sand. Géotechnique 52(4): 299-304. DOI: 10.1680/geot.2002.52.4.299

McDowell GR, de Bono JP (2013) On the micro mechanics of one-dimensional normal compression. Géotechnique 63(11): 895-908. DOI: 10.1680/geot.12.P.041

McDowell GR, de Bono JP (2013) DEM of triaxial tests on crushable sand. Granular Matter 16(4): 551-562. DOI: 10.1007/ s10035-014-0500-x

Munjiza A, Owen DRJ, Bicanic N (1995) A combined finite-discrete element method in transient dynamics of fracturing solids. Engineering Computations 12(2): 145-174. DOI: 10.1108/02644409510799532

Munjiza A (2004) The combined finite-discrete element method. Wiley, Chichester, U.K. DOI: 10.1002/0470020180

Owen DRJ, Feng YT, Neto EAD, et al. (2004) The modelling of multi-fracturing solids and particulate media. International Journal for Numerical Methods in Engineering 60(1): 317-339. DOI: 10.1002/nme.964

Qian JG, Huang, MS, Sun HZ (2011). Macro-micromechanical approaches for non-coaxiality of coarse grained soils. Science China-Technological Sciences 54(s1):147-153. DOI: 10.1007/ s11431-011-4634-3

Qian JG, You ZP, Huang MS, GU XQ (2013a) A micromechanics-based model for estimating localized failure with effects of fabric anisotropy. Computers and Geotechnics 50:90-100. DOI: 10.1016/j.compgeo.2013.01.001

Qian JG, You ZP, Huang MS (2013b) Anisotropic characteristics of granular materials under simple shear. Journal of Central South University 20(8):2275-2284. DOI: 10.1007/s11771-013-1734-1

Robertson D (2000) Computer simulations of crushable aggregates. PhD dissertation, Cambridge University, UK.

Thornton C (2000) Numerical simulations of deviatoric shear deformation of granular media. Géotechnique 50(1): 43-53. DOI: 10.1680/geot.2000.50.1.43

Tsoungui O, Vallet D, Charmet JC (1999) Numerical model of crushing of grains inside two-dimensional granular materials. Powder Technology 105(1): 190-198. DOI: 10.1016/S0032-5910(99)00137-0

Ueda TM, Yamada Y (2013) DEM simulation on the one-dimensional compression behavior of various shaped crushable granular materials. Granular Matter 15(5): 675-684. DOI: 10.1007/s10035-013-0415-y

Wang J, Yan H (2011) 3D DEM Simulation of Crushable Granular Soils under Plane Strain Compression Condition. Procedia Engineering. 14: 1713-1720. DOI: 10.1016/j.proeng.2011.07.215

Wang J, Yan H (2013) On the role of particle breakage in the shear failure behavior of granular soils by DEM. International Journal for Numerical and Analytical Methods in Geomechanics 37(8): 832-854. DOI: 10.1002/nag.1124

Weibull W (1951) A statistical distribution function of wide applicability. Journal of Applied Mechanics 18: 293-297.

Wichtmann T, Niemunis A, Triantafyllidis TH (2007) Strain accumulation in sand due to cyclic loading: drained cyclic tests with triaxial extension. Soil Dynamics and Earthquake Engineering 27(1): 42-48. DOI: 10.1016/j.soildyn.2006.04.001

Xiang J, Munjiza A and Latham JP (2009) Finite strain, finite rotation quadratic tetrahedral element for the combined finite-discrete element method. International Journal for Numerical Methods in Engineering 79(8): 946-978. DOI: 10.1002/ nme.2599

Zhou W, Ma G, Chang XL, et al. (2015) Discrete modeling of rockfill materials considering the irregular shaped particles and their crushability. Engineering Computations 32(4): 1104-1120. DOI: 10.1108/EC-04-2014-0086